Kovove Mater. 51 2013 89–99
DOI: 10.4149/km_2013_2_89

Effect of solidification parameters on microsegregation behaviour of main alloying elements in a peritectic TiAl-based alloy

A. Klimová[1,2]*, J. Lapin[1], T. Pelachová[1], M. Nosko[1]

[1] *Institute of Materials and Machine Mechanics, Slovak Academy of Sciences, Račianska 75, 831 02 Bratislava 3, Slovak Republic*
[2] *Institute of Materials Science, Faculty of Materials Science and Technology in Trnava, Slovak University of Technology in Bratislava, Paulínska 16, 917 24 Trnava, Slovak Republic*

Received 22 April 2013, received in revised form 20 May 2013, accepted 20 May 2013

Abstract

The effect of solidification parameters, such as growth rate V and temperature gradient G_L, on microsegregation behaviour of main alloying elements in peritectic Ti-44Al-5Nb-0.2B-0.2C (at.%) alloy was studied. Samples for microsegregation study were prepared by quench during directional solidification (QDS) at various combinations of V and G_L. The studied alloy solidifies with β (Ti-based solid solution with cubic crystal structure) primary solidification phase and undergoes $L + \beta \rightarrow \alpha$ peritectic transformation. The energy-dispersive spectrometry (EDS) analyses and calculated effective distribution coefficients k_{eff} for Al, Ti and Nb confirm that the alloying elements such as Ti and Nb segregate predominantly into the β dendrites and Al into the interdendritic liquid during directional solidification. Formation of the peritectic α-phase (Ti-based solid solution with hexagonal crystal structure) leads to an intensive back-diffusion of the alloying elements. Boron segregates into interdendritic liquid where it forms (Ti, Nb)B particles with ribbon-like morphology. Severity of microsegregation expressed by segregation deviation parameter σ_m^{Al} for aluminium decreases with increasing growth rate V in the mushy zone and only slightly increases below the mushy zone. Moderate decrease of σ_m^{Al} with the increase of G_L is observed at all measured positions except the position located close to the dendrite tip.

K e y w o r d s: titanium aluminides, TiAl, solidification, energy-dispersive spectrometry, microsegregation

1. Introduction

In the recent years intermetallic TiAl-based alloys have been used for demanding applications in power engineering, aircraft and automotive industry, especially for processing of low pressure turbine blades for stationary gas turbines and aircraft engines and turbocharger wheels for petrol and diesel engines [1–3].

Coarse-grained microstructure, casting texture and significant chemical inhomogeneity of cast components from TiAl-based alloys are detrimental to their mechanical properties. However, the proper selection of alloying elements leads to a significant grain refinement of the microstructure. Majority of TiAl-based alloys containing of about 44–45 at.% of Al and 5–10 at.% of Nb solidify through β-phase (Ti-based solid solution with cubic crystal structure), which transforms to α-phase (Ti-based solid solution with hexagonal crystal structure) during cooling. Formation of the α-phase from the β-phase is a complex problem, because the α-phase can be formed either through peritectic reaction and transformation in peritectic type alloys, or by solid state transformation from single β-phase resulting in the formation of different crystallographic orientation variants of the α-phase. The effect of peritectic reaction, which is part of the solidification path, is rather harmful for the grain refining process [4]. Therefore, the basic ternary systems are further alloyed by carbon and boron, which promote grain refinement [5]. Low addition of boron increases

*Corresponding author: tel.: +421 2 49268304; fax. +421 2 49268312; e-mail address: ummsakli@savba.sk

Table 1. Parameters of the directional solidification

Sample No.	Maximum melt temperature (°C)	Growth rate V (10^{-5} m s^{-1})	Temperature gradient G_L (10^3 K m^{-1})	G_L/V (10^8 K m^{-2} s)
958	1650	1.39	3	2.16
962	1650	2.78	3	2.88
961	1650	11.8	3	3.60
960	1680	1.39	4	1.08
952	1680	2.78	4	1.44
957	1680	11.8	4	1.80
956	1720	1.39	5	0.25
948	1720	2.78	5	0.34
951	1720	11.8	5	0.42

the rate of heterogeneous nucleation of the α-phase during $\beta \rightarrow \alpha$ transformation leading to fine grain structure of the alloy. Nb, B and C increase stability of the α grains against their growth on passing through the α single-phase field during cooling [6]. In addition, small amount of C improves high-temperature tensile and creep strength of these alloys [6]. Due to the beneficial effects of these elements on the grain refinement and mechanical properties, peritectic Ti-44Al-5Nb-0.2B-0.2C (at.%) alloy has been designed for structural applications that demand high temperature strength and good oxidation and creep resistance of cast components [4]. Despite the fact that the effect of above mentioned alloying elements on the grain formation has been already studied in several β solidifying TiAl-based alloys [7–9], description of microsegregation behaviour of main alloying elements in peritectic type alloys during solidification at different solidification conditions is still lacking [10], especially in relation to the investigations of the columnar to equiaxed transition in TiAl-based alloys [11].

The aim of this paper is to study the effect of solidification parameters such as growth rate V and temperature gradient G_L on microsegregation behaviour of main alloying elements (Ti, Al and Nb) in peritectic Ti-44Al-5Nb-0.2B-0.2C (at.%) alloy. Quench during directional solidification (QDS) experiments were carried out to prepare samples at various V and G_L, to identify primary solidification phase, solidification path and describe microsegregation behaviour of main alloying elements in this alloy during solidification.

2. Experimental procedure

The intermetallic alloy with the nominal composition Ti-44Al-5Nb-0.2B-0.2C (at.%) and oxygen content of about 500 wt ppm was supplied in the form of vacuum arc re-melted conical ingot with a diameter changing from 35 to 60 mm and length of 310 mm. The ingot was cut to small rectangular blocks with dimensions of $11 \times 11 \times 150$ mm^3 by electro spark machining. Cylindrical samples for QDS experiments with a diameter of 10 mm were lathe machined from the blocks. Directional solidification was performed in dense cylindrical Y_2O_3 moulds with inside/outside diameter of 10/15 mm and length of 170 mm at nine combinations of three constant growth rates V and three constant temperature gradients in liquid at the solid-liquid interface G_L, as summarized in Table 1. The effect of Y_2O_3 moulds on contamination of TiAl-based alloy during directional solidification has been described recently by Lapin et al. [12]. Directional solidification was performed in a modified Bridgman-type apparatus described elsewhere [13]. After directional solidification to a constant length of 80 mm the samples were quenched by a rapid displacement of the mould into the water-cooled crystallizer at a cooling rate of 50 K s^{-1}.

Microstructural investigations were performed by optical microscopy (OM), backscattered scanning electron microscopy (BSEM) and X-ray diffraction (XRD). Chemical composition and distribution of main alloying elements was measured by energy-dispersive spectrometry (EDS). OM, BSEM, XRD and EDS samples were prepared using standard grinding and polishing metallographic techniques. After mechanical polishing the samples for optical microscopy were chemically etched in a reagent of 100 ml H_2O, 10 ml HNO_3 and 3 ml HF. For EDS area and point analyses along a line, JSM-7600F scanning electron microscope with EDS detector was used. Before each measurement, the quant optimization on Ti and standardization using a standard with nominal composition Ti-46Al-8Nb (at.%) were performed. The preparation of homogeneous standards for calibration of EDS equipment was described elsewhere [14]. Accelerating voltage during all measurements was 10 kV. According to Monte Carlo simulation of electron trajectory in the studied alloy the predicted signal depth at 10 kV is around 700–800 nm. Volume fraction of solid was measured by computerized image analysis on BSEM micrographs taken from the mushy zone of QDS samples.

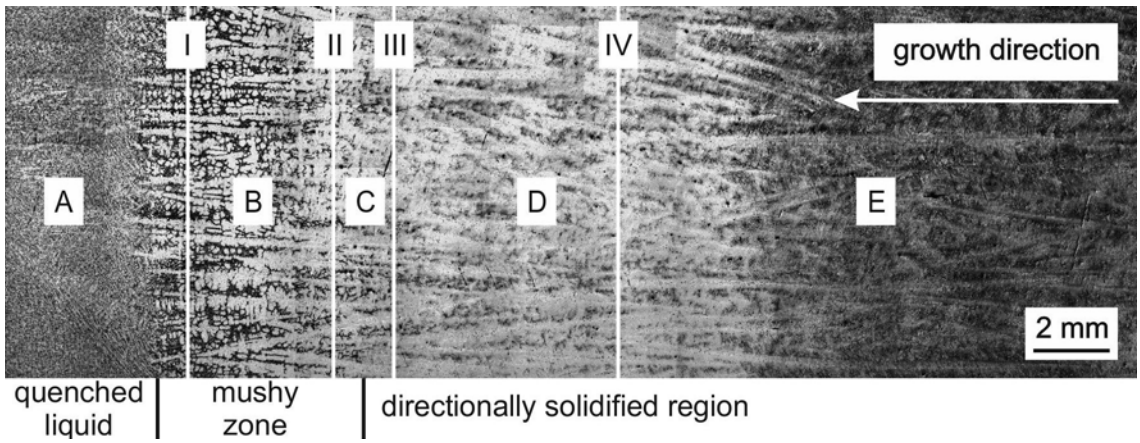

Fig. 1. OM micrograph of the longitudinal section of the QDS sample prepared at $V = 1.39 \times 10^{-5}$ m s^{-1} and $G_L = 5000$ K m^{-1}.

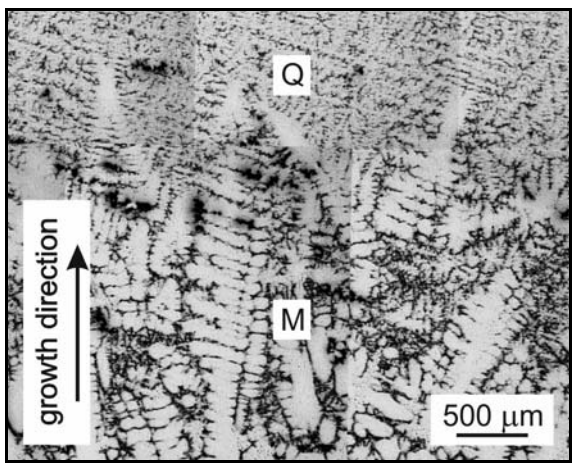

Fig. 2. "Seaweed" morphology of dendrites on the quenched solid-liquid interface in the QDS sample prepared at $V = 2.78 \times 10^{-5}$ m s^{-1} and $G_L = 4000$ K m^{-1}, (OM): Q – quenched liquid; M – mushy zone.

3. Results

3.1. Microstructure of the QDS samples

The QDS experiments used in the present work allowed preserving the most remarkable microstructure features along the solidification path of the studied alloy. Figure 1 shows the typical microstructure on the longitudinal section of the QDS samples. Despite the fact that the dendrites are slightly disoriented from the direction parallel to the growth direction and show the typical "seaweed" morphology (Fig. 2), orthogonal orientation of the secondary dendrites arms to the primary arms indicates that the primary solidification phase has a cubic crystal structure. This is in a good agreement with Ti-Al phase diagram [5], where the primary solidification phase in the composition range around 44 at.% Al is the β-phase. Figure 3 shows XRD patterns taken from the regions A, B, C, D and E (Fig. 1) indicating presence of following phases: β, α, γ(TiAl), α_2(Ti_3Al), (Ti, Nb)B and Y_2O_3. The typical microstructure of the mushy zone is shown in Fig. 4. As the solidification continues, formation of α-phase envelope around the β dendrites through a peritectic reaction $L + \beta \rightarrow \alpha$ is observed (Fig. 5). Evidence for the formation of the α-phase around the β dendrites is found at the distance of about 4–6 mm (in dependence of the QDS parameters) from the quenched solid-liquid interface. The peritectic α-phase forms at the expense of the β dendrites and the interdendritic liquid and can be distinguished on BSEM micrographs as a darker grey layer delimited by the network of the β-phase on the dendrite site and black coloured interdendritic γ(TiAl)-phase. However, the β-phase within the dendrites is highly unstable during quenching and transforms to the α-phase with a residual network of the β-phase (white coloured phase in Fig. 5). At lower temperatures, the microstructure undergoes fast homogenization and consists of the α/α_2 matrix with some fine γ lamellae, residual β-phase (R(β)) and Y_2O_3 particles (Fig. 6). From the distance of 15–17 mm (in dependence of the QDS parameters) from the quenched solid-liquid interface the fully lamellar $\alpha_2 + \gamma$ microstructure can be observed, as shown in Fig. 7. Figure 8 shows (Ti, Nb)B borides with metastable *oC8* (B_f) structure and ribbon-like morphology formed in the interdendritic region. Formation of the (Ti, Nb)B borides is in the agreement with the recent observations of Hecht et al. [4]. Based on the microstructural analysis the following solidification and solid phase transformation sequences are proposed for the studied alloy:

$$L \rightarrow L + \beta \rightarrow \beta + \alpha \rightarrow \alpha + (Ti, Nb)B + R(\beta) \rightarrow \\ \rightarrow \alpha + \gamma + (Ti, Nb)B \rightarrow \alpha_2 + \gamma + (Ti, Nb)B.$$

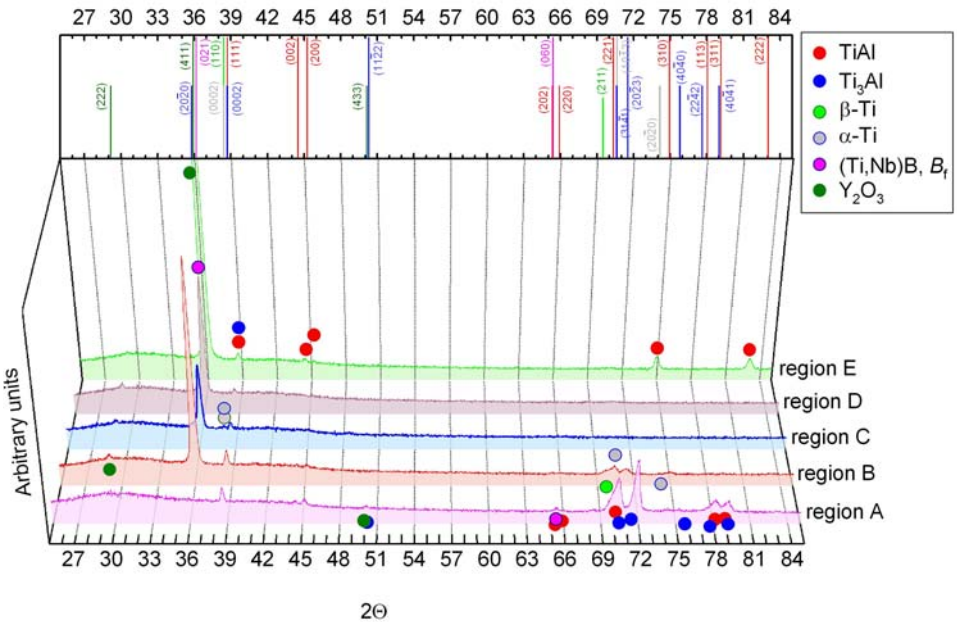

Fig. 3. XRD patterns taken from the regions A, B, C, D and E marked in Fig. 1: $V = 2.78 \times 10^{-5}$ m s^{-1} and $G_L = 5000$ K m^{-1}.

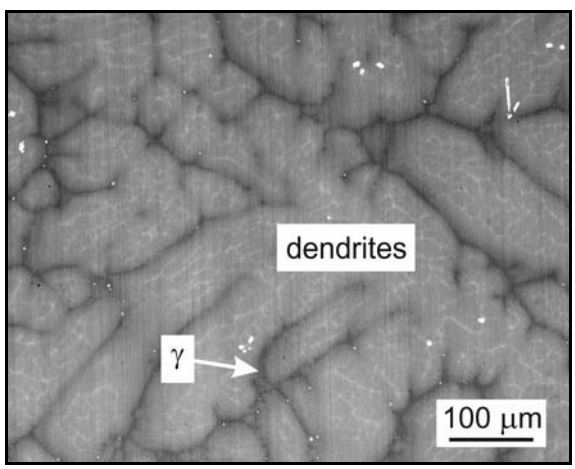

Fig. 4. Dendritic microstructure of the mushy zone (BSEM): $V = 2.78 \times 10^{-5}$ m s^{-1} and $G_L = 5000$ K m^{-1}.

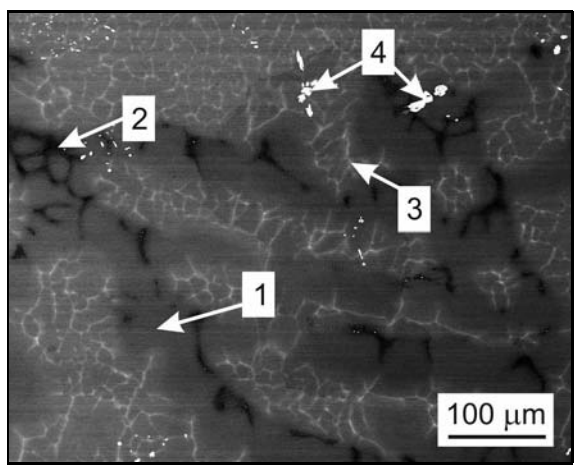

Fig. 5. Formation of the α-phase envelope around the β dendrites through a peritectic reaction in the QDS sample prepared at $V = 2.78 \times 10^{-5}$ m s^{-1} and $G_L = 5000$ K m^{-1}, (BSEM): 1 – peritectic α-phase; 2 – γ-phase; 3 – network of β-phase; 4 – Y_2O_3 particles.

3.2. Microsegregation behaviour of Al, Ti and Nb

Microsegregation behaviour of the main alloying elements during directional solidification was investigated on the longitudinal sections of the QDS samples at four positions with different distance from the dendrite tip. Figure 1 shows these analysed positions marked as I, II, III and IV, which correspond to fraction of solid f_s of (80 ± 2) vol.%, (90 ± 3) vol.%, 100 vol.% and 100 vol.%, respectively. Each EDS profile consists of 100 individual measurements positioned by 20 µm of each other along a line (Fig. 9). To refine specific regions of distribution curves, additional measurements along the line with a length ranging from 20 to 30 µm were performed within the interdendritic region and dendrites, as illustrated in Fig. 10.

Data from EDS measurements at the positions I, II, III and IV were sorted using single-element sorting scheme with Al as the main sorting element [15]. Cumulative fraction $f(i)$ was assigned to each measured point i. Since absolute maximum and minimum concentrations cannot be guaranteed for the sample using

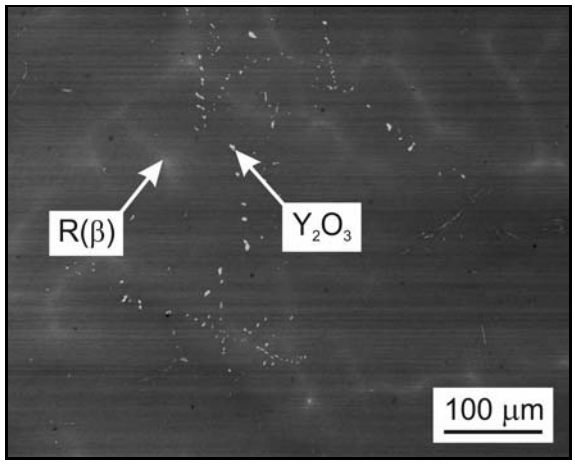

Fig. 6. Residual β-phase and Y_2O_3 particles below the mushy zone (BSEM): $V = 2.78 \times 10^{-5}$ m s^{-1} and $G_L = 5000$ K m^{-1}.

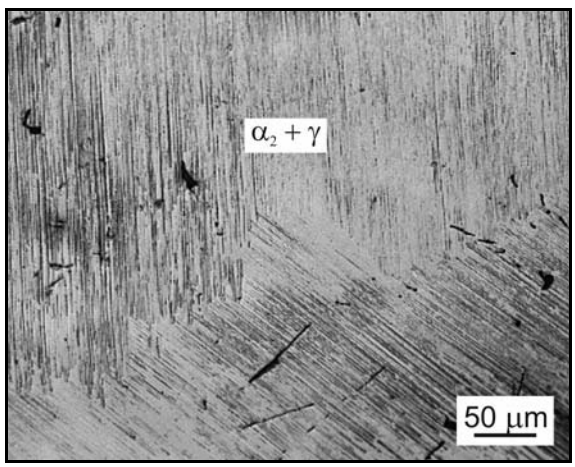

Fig. 7. Fully lamellar $\alpha_2 + \gamma$ microstructure below the mushy zone (OM): $V = 2.78 \times 10^{-5}$ m s^{-1} and $G_L = 4000$ K m^{-1}.

random sampling, cumulative fraction was assigned to [15]:

$$f(i) = (R_i - 0.5)/N, \tag{1}$$

where R_i is the rank number and N is the total number of points. Hence, $f(i)$ continuously varies from 0 to 1 ($0 < f(i) < 1$).

Figure 11 shows the typical evolutions of the concentration of Ti, Al and Nb with cumulative fraction at all four positions. The solidification between the positions I and II leads to the pronounced microsegregation of main alloying elements. A strong back-diffusion between positions II and III indicates the beginning of the peritectic reaction. The concentration profiles in the position IV reflect intensive homogenization of the alloy during solidification caused by several

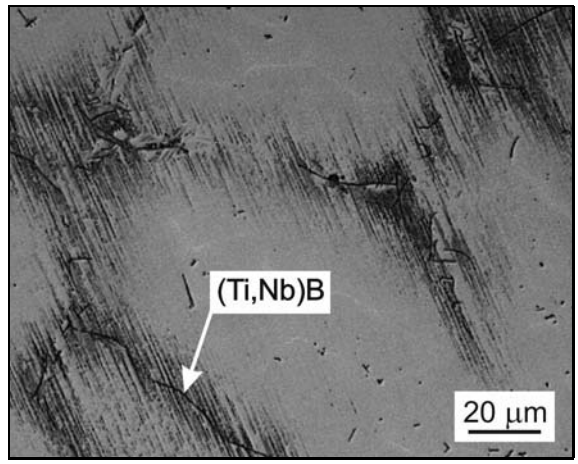

Fig. 8. Formation of (Ti, Nb)B particles with the ribbon-like morphology within the interdendritic region (OM): $V = 2.78 \times 10^{-5}$ m s^{-1} and $G_L = 5000$ K m^{-1}.

liquid-solid and solid-solid phase transformations.

For quantitative evaluation of severity of microsegregation, segregation deviation parameter σ_m^j was calculated for each alloying element j at the positions I, II, III and IV according to relationship [16]:

$$\sigma_m^j = \frac{1}{NC_0^j} \sum_{i=1}^{N} |C_i^j - C_0^j|, \tag{2}$$

where C_0^j is the average concentration of the element j, C_i^j is the concentration of the element j at the point i and N is the total number of the analysed points for one analysed position. The parameter σ_m^j has no limitation of other microsegregation parameters such as segregation range and segregation coefficient, which are based only on the minimum and maximum solute concentrations because it is calculated from all measured data at the analysed position [17]. Figure 12 shows the variations of segregation deviation parameter σ_m^{Al} for Al with the growth rate and temperature gradient at all four positions. It should be noted that the segregation deviation parameters σ_m^{Ti} and σ_m^{Nb} for Ti and Nb, respectively, showed similar variations with V and G_L as that of σ_m^{Al} presented in Fig. 12.

3.3. Distribution coefficients of Al, Ti and Nb

Distribution coefficient $k^{s/l}$ belongs to the basic quantities characterizing the segregation behaviour of the alloying element during solidification. There are several different approaches to the calculation of the distribution coefficient. Under real solidification conditions, when the equilibrium state is unreachable, instead of equilibrium distribution coefficient effective distribution coefficient k_{eff} is calculated. One method for calculation of k_{eff} uses the Gulliver-Scheil analysis,

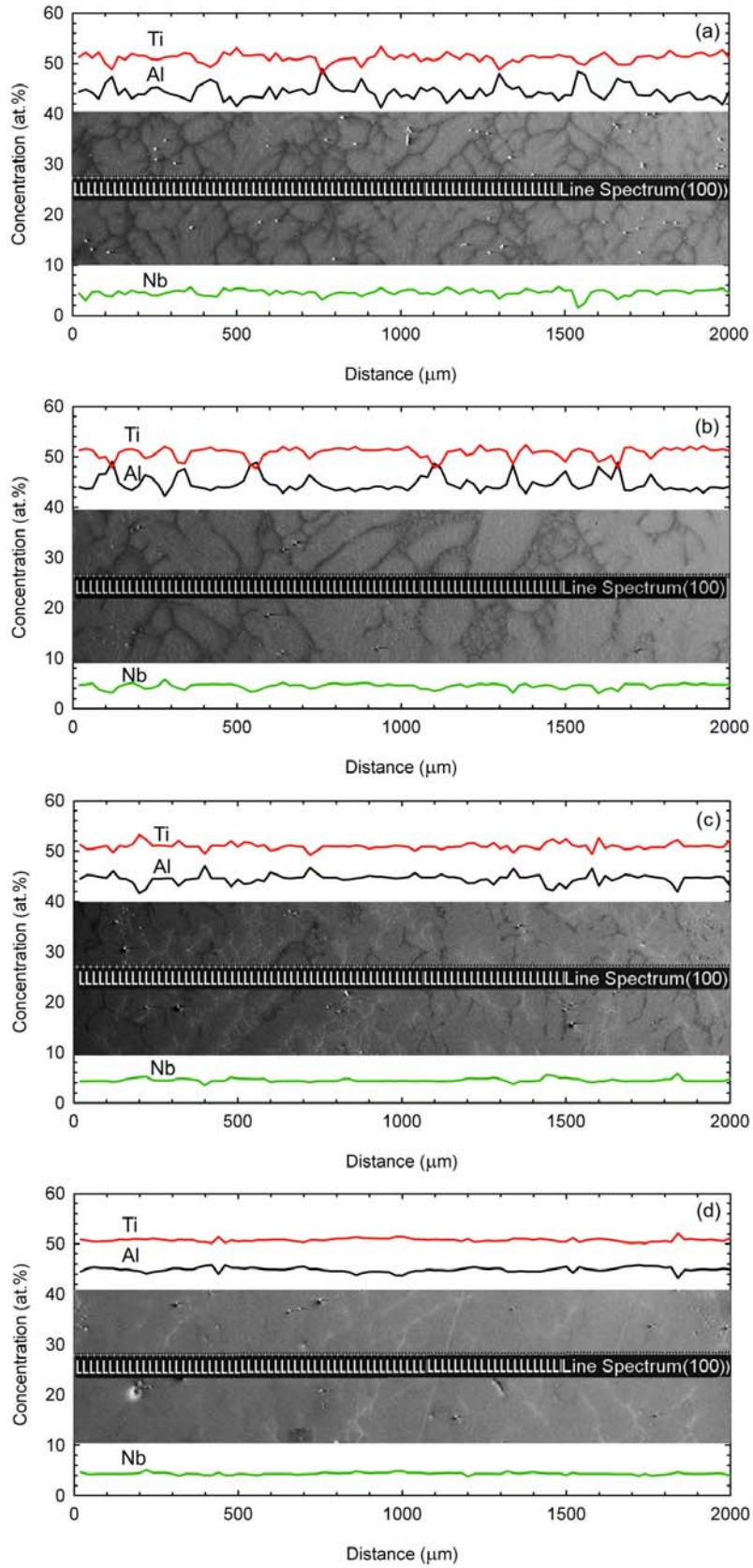

Fig. 9. SEM micrographs and corresponding EDS profiles of Ti, Al and Nb in the position I (a), II (b), III (c) and IV (d) of the QDS sample prepared at $V = 2.78 \times 10^{-5}$ m s^{-1} and $G_L = 5000$ K m^{-1}.

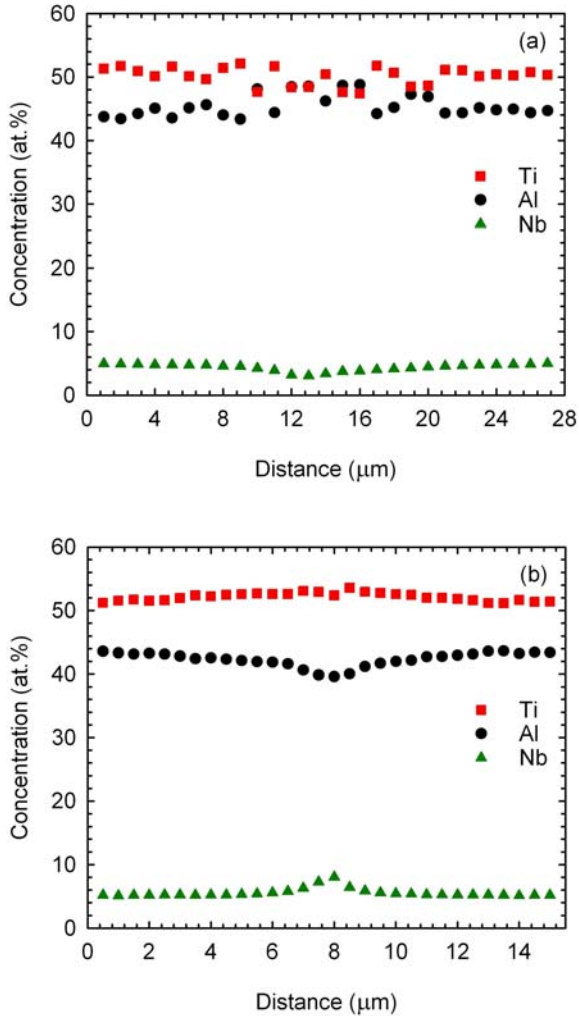

Fig. 10. Distribution of Ti, Al, and Nb in the sample prepared at $V = 2.78 \times 10^{-5}$ m s^{-1} and $G_L = 4000$ K m^{-1}: (a) within interdendritic region and (b) within dendrite.

where solute concentration relative to the initial concentration is determined for a few values of the cumulative fraction and k_{eff} is then estimated from the log-log plot of the Gulliver-Scheil equation [18]. The second method for calculation of k_{eff} uses the evolution of the concentrations of the alloying element with the cumulative fraction, where the ratio of the first 10 points of the concentration profile measured at the dendrite tip to the initial or average composition is calculated [19]. The third method for calculation of k_{eff} includes whole set of the concentration data of the measured profile as is described in [20]. For the comparison with the data reported by Charpentier et al. [17], distribution coefficients for Al, Ti and Nb are calculated also as a ratio of the average concentrations of alloying elements within the dendrites and interdendritic regions in the mushy zone close to the dendrite tip. The average k_{eff} for Ti, Al and Nb calculated

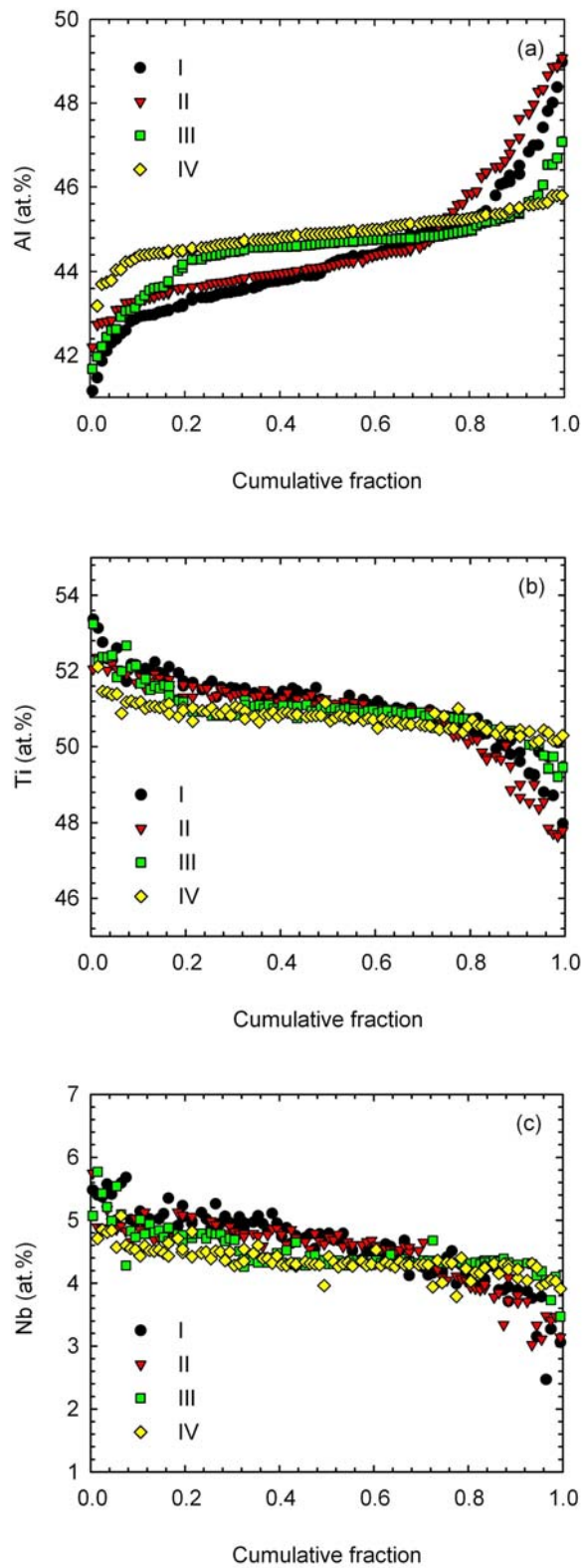

Fig. 11. Evolutions of the concentration of main elements with cumulative fraction in four measured positions of the QDS sample prepared at $V = 2.78 \times 10^{-5}$ m s^{-1} and $G_L = 5000$ K m^{-1}: (a) Al, (b) Ti and (c) Nb.

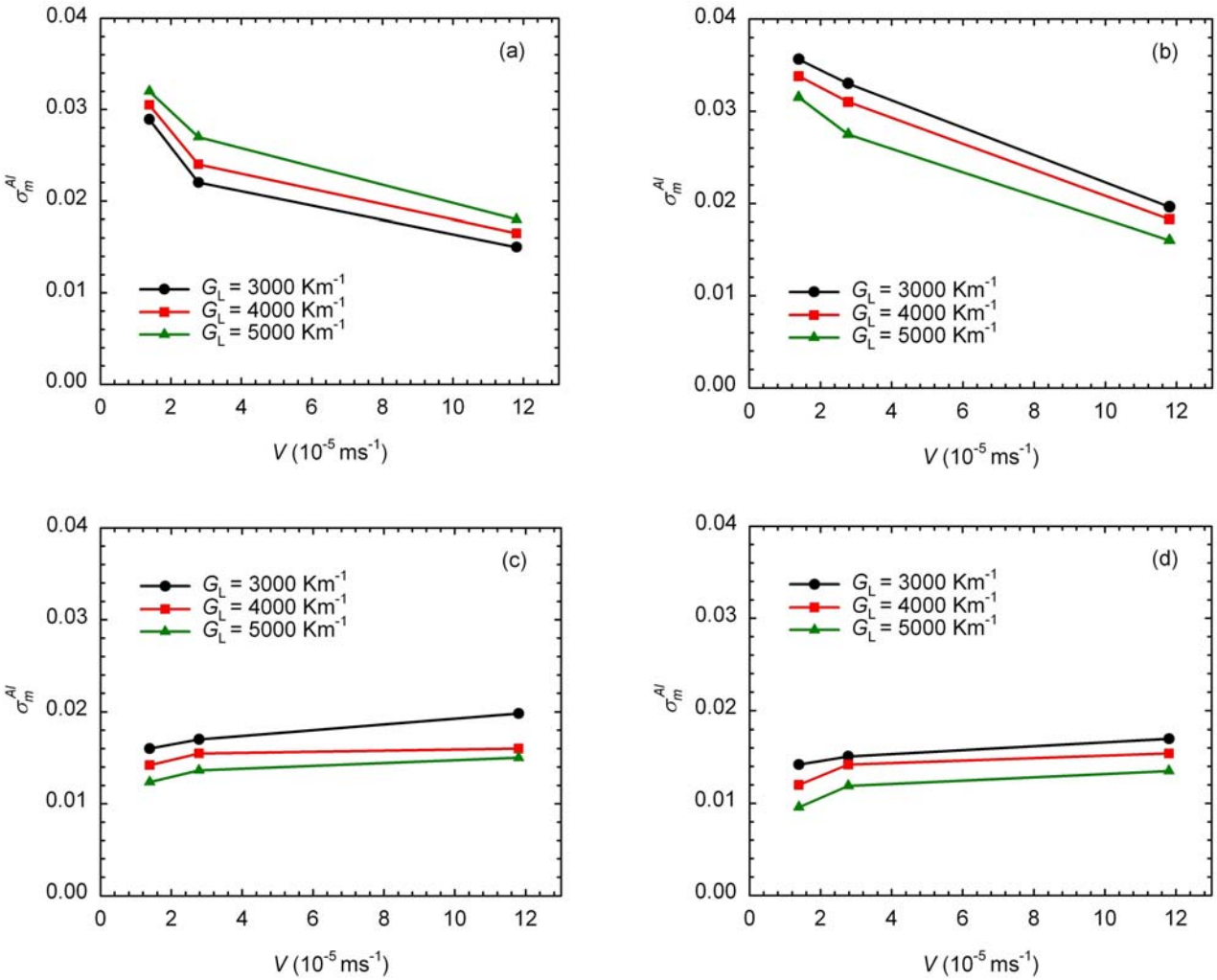

Fig. 12. Variations of the segregation deviation parameter $\sigma_{\mathrm{m}}^{\mathrm{Al}}$ with the growth rate V in the positions I (a), II (b), III (c) and IV (d) at three constant temperature gradients G_{L}. The temperature gradients are indicated in the figure.

by the above mentioned methods are summarized in Table 2 and compared with distribution coefficients estimated from multipoint analysis grids using electron probe micro-analyzer (EPMA) for Ti-48Al-2Cr-2Nb (at.%) alloy [17]. It should be noted that for calculations of k_{eff} of the studied alloy, EDS profiles of Al, Ti and Nb close to the dendrite tip (position I) are used.

4. Discussion

4.1. Morphology of solid-liquid interface

Most metals solidify into wide range of morphologies, including dendritic, seaweed, dense-branched, fractal-like and some that are a continuous variation between these patterns. As shown in Fig. 2, the β primary solidification phase is growing in the studied alloy with the so-called seaweed morphology. Generally, seaweed structures are formed in metallic systems at sufficiently high undercoolings of the melt and sufficiently low anisotropy of the surface free energy of the solid-liquid interface [21], through successive tip splitting of primary branches on the solidification front [22]. The dendrite-to-seaweed transition occurs as the curvature contribution of the tip undercooling, which increases with growth rate, becomes comparable to the solutal undercooling, leading to the alternating tip splitting and change of the tip growth direction [23]. The transition from dendrite to seaweed is highly dependent on the anisotropy strength and material parameters, and shifts to much higher growth rates for large anisotropic systems. The effect of growth rate and temperature gradient on the formation of the seaweed structure in metallic materials with cubic crystal structure, where the imposed temperature gradient is misaligned with respect to the main axes of the crystalline structure, was numerically and also experimentally investigated on directionally solidified Mg-Al alloys by Amoorezaei at al. [24]. It was shown

Table 2. Calculations of effective distribution coefficients k_{eff} for Ti, Al and Nb using different methods

	$k_{\mathrm{eff}}^{\mathrm{Ti}}$	$k_{\mathrm{eff}}^{\mathrm{Al}}$	$k_{\mathrm{eff}}^{\mathrm{Nb}}$
Ti-44Al-5Nb-0.2B-0.2C (at.%)			
Gulliver-Scheil analysis	1.02 ± 0.01	0.95 ± 0.01	1.15 ± 0.03
Gulliver-Scheil fit	1.02	0.96	1.11
Ratio of first 10 points to the average composition	1.02 ± 0.01	0.96 ± 0.01	1.15 ± 0.03
Ratio of first 10 points to the initial composition	1.03 ± 0.01	0.95 ± 0.01	1.16 ± 0.03
Processing of the whole set of the concentration data measured at the dendrite tip	1.02 ± 0.01	0.97 ± 0.01	1.11 ± 0.06
Ratio of the average concentrations within dendrites and interdendritic region	1.04 ± 0.01	0.92 ± 0.02	1.41 ± 0.11
Ti-48Al-2Cr-2Nb (at.%) [11]			
Ratio of the average concentrations within dendrites and interdendritic regions	1.14 ± 0.04	0.86 ± 0.02	1.42 ± 0.14
Gulliver-Scheil fit	–	0.92	1.17

that at the growth rates just above the planar-cellular instability, cells grow in the direction of the temperature gradient. As the growth rate increases towards the cell-to-dendrite transition, cells begin to deviate towards the preferred crystallographic direction until the primary dendrite arms grow along a main crystalline axis, in agreement with the findings of Trivedi et al. [25]. In the dendritic region, lower temperature gradients favour growth along the direction of the main crystalline axes, whereas higher thermal gradient favour a seaweed microstructure where dendrites tips continuously split and change orientation. The thermal gradient required to favour seaweed structures increases with increasing growth rate.

4.2. Effect of the solidification parameters on microsegregation

As is shown in Fig. 1, positions I and II are located in the mushy zone and positions III and IV below the mushy zone. Position I is situated close to the dendrite tip ($f_{\mathrm{s}} = 80$ vol.%) and position III close to the position of the peritectic transformation ($f_{\mathrm{s}} = 100$ vol.%), which leads to a strong back-diffusion of the alloying elements [26]. The growth rate V and temperature gradient G_{L} affect the distribution of the alloying elements differently within and below the mushy zone. Severity of microsegregation decreases with increasing growth rate in the mushy zone (positions I and II) and only slightly increases below the mushy zone (positions III and IV) at all three studied temperature gradients (Fig. 12). Decrease of $\sigma_{\mathrm{m}}^{\mathrm{Al}}$ with the increasing V in the mushy zone is in a good agreement with the model based on the measured temperature curves proposed by Martorano and Capocchi [16]. In this model, similar dependence is predicted also for the region below the mushy zone. However, lower $\sigma_{\mathrm{m}}^{\mathrm{Al}}$ at lower growth rates in positions III and IV are observed in our case. This phenomenon can be explained by the extensive homogenization of the studied alloy during solid state transformations when the growth rate is reduced. This is in agreement with microsegregation model of Brody and Flemings [27] and also with the model based on a constant average cooling rate of Martorano and Capocchi [16].

The temperature gradient affects the microsegregation of alloying elements in the same way as the growth rate at the positions II, III and IV, where moderate decrease of $\sigma_{\mathrm{m}}^{\mathrm{Al}}$ with the increase of G_{L} is observed at all applied growth rates (Figs. 12b,c,d). On the other hand, there is an inverse tendency at the position I, as shown in Fig. 12a. According to Martorano and Capocchi [16], the value of σ_{m}^{j} is initially zero because the liquid is assumed to be homogeneous before the beginning of the solidification of peritectic alloys and this value increases to a maximum due to solute partitioning during solidification. However, there is no clear influence of different cooling rates or temperature gradients on σ_{m}^{j} predicted for early stages of the solidification [16]. The observed increase of $\sigma_{\mathrm{m}}^{\mathrm{Al}}$ with the increase of G_{L} at the position I leads to the assumption, that the increase of $\sigma_{\mathrm{m}}^{\mathrm{Al}}$ at the beginning of the solidification is slightly faster at higher G_{L} in the studied alloy.

4.3. Distribution coefficients of Al, Ti and Nb

As is seen in Table 2, the value of the effective distribution coefficient for Nb higher than 1 calculated by the applied methods confirms the strong partitioning of this element to the β dendrites, while the value of the effective distribution coefficient for Al lower than 1 indicates its partitioning to the interdendritic liquid during directional solidification. There is the negligible difference between distribution coefficients for Ti calculated by the applied methods. Values of distribution coefficients calculated as a ratio of the average concentrations of alloying elements within the dend-

rites and interdendritic regions are slightly lower for Al and higher for Nb than the values calculated by other methods. Despite of a good agreement between the values estimated from Gulliver-Scheil fit and those resulting from other methods, it should be noted, that Gulliver-Scheil analysis [18] is not sufficiently accurate for real systems, because it assumes complete diffusion in the liquid phase and no diffusion in the solid phase. The Gulliver-Scheil equation does not adequately estimate the initial and especially final solute concentration. Due to this limitation, the determination of the distribution coefficient from fitting of the experimental data with the plot of Gulliver-Scheil equation is only approximate. Therefore, also values marked as Gulliver-Scheil analysis in Table 2 were calculated not for a few values of f as proposed by Glicksman [18], but for much higher cumulative fraction ($f = 0.5$). Estimation of k_{eff} from Gulliver-Scheil analysis using solute concentrations for only first few values of f leads to much lower values of distribution coefficient for Al and much higher for Nb and Ti than those listed in Table 2.

5. Conclusions

The investigation of the effect of solidification parameters on the microsegregation behaviour of main alloying elements in a peritectic Ti-44Al-5Nb-0.2B-0.2C (at.%) alloy can be summarized as follows:

1. The alloy solidifies with the β primary solidification phase with "seaweed" type of dendritic morphology. The proposed solidification path includes the peritectic transformation L + $\beta \rightarrow \alpha$ and formation of (Ti, Nb)B borides with metastable *oC8* (B_f) structure and ribbon-like morphology predominantly in the interdendritic region.

2. Severity of microsegregation expressed by segregation deviation parameter σ_m^{Al} for aluminium decreases with increasing growth rate V in the mushy zone and only slightly increases below the mushy zone at the studied temperature gradients G_L. Moderate decrease of σ_m^{Al} with the increase of G_L is observed at all measured positions except the position located close to the dendrite tip at the studied V where the inverse tendency is observed.

3. The calculated effective distribution coefficients k_{eff} for Al, Ti and Nb confirm the preferential segregation of Nb and Ti into the β dendrites and Al into the interdendritic liquid during directional solidification. There are only negligible differences among distribution coefficients for Ti calculated by different methods applied in this work. Values of k_{eff} calculated as a ratio of the average concentrations of alloying elements within the dendrites and interdendritic regions are slightly lower for Al and higher for Nb than the values calculated by other applied methods.

Acknowledgements

The financial support of the Slovak Research and Development Agency under the contract APVV-0434-10 and the Slovak Grant Agency for Science under the contract VEGA 2/0149/13 is acknowledged. One of the authors (J. Lapin) would like to acknowledge the support of the RMTVC project under the contract No. CZ.1.05/2.1.00/01.0040.

References

[1] Lapin, J.: In: Technológia 2011. Bratislava, STU 2011, p. 3.
[2] Lapin, J.: Kovove Mater., *43*, 2005, p. 81.
[3] Lapin, J., Pelachová, T.: Kovove Mater., *42*, 2004, p. 143.
[4] Hecht, U., Witusiewitz, V., Drevermann, A., Zollinger, J.: Intermetallics, *16*, 2008, p. 969. doi:10.1016/j.intermet.2008.04.019
[5] Eiken, J., Apel, M., Witusiewicz, V. T., Zollinger, J., Hecht, U.: J. Phys. – Condens. Mat., *21*, 2009, 464104 (7pp). doi:10.1088/0953-8984/21/46/464104
[6] Imayev, R. M., Imayev, V. M., Oehring, M., Appel, F.: Intermetallics, *15*, 2007, p. 451. doi:10.1016/j.intermet.2006.05.003
[7] Hecht, U., Daloz, D., Lapin, J., Witusiewicz, V. T., Zollinger, J.: In: Mater. Res. Soc. Symp. Proc., Materials Research Society. Eds.: Palm, M., Bewlay, B. P., Takeyama, M., Wiezorek, J. M. K., He, Y.-H. Warrendale, PA 2009, no. 1128-U03-01.
[8] Hu, D., Yang, C., Huang, A., Dixon, M., Hecht, U.: Intermetallics, *23*, 2012, p. 49. doi:10.1016/j.intermet.2011.12.022
[9] Hu, D., Yang, C., Huang, A., Dixon, M., Hecht, U.: Intermetallics, *23*, 2012, p. 68. doi:10.1016/j.intermet.2011.12.008
[10] Daloz, D., Hecht, U., Zollinger, J., Combeau, H., Hazotte, A., Zaloznik, M.: Intermetallics, *19*, 2011, p. 749. doi:10.1016/j.intermet.2010.11.013
[11] Lapin, J., Gabalcová, Z.: Intermetallics, *19*, 2011, p. 797. doi:10.1016/j.intermet.2010.11.021
[12] Lapin, J., Gabalcová, Z., Pelachová, T.: Intermetallics, *19*, 2011, p. 396. doi:10.1016/j.intermet.2010.11.007
[13] Lapin, J., Ondrúš, Ľ., Nazmy, M.: Intermetallics, *10*, 2002, p. 1019. doi:10.1016/S0966-9795(02)00119-X
[14] Klimová, A.: In: 7th Seminar of Central European PhD Students – Research in Materials Science. Trnava 2012.
[15] Ganesan, M., Dye, D., Lee, P. D.: Metall. Mater. Trans. A, *36A*, 2005, p. 2191. doi:10.1007/s11661-005-0338-2
[16] Martorano, M. A., Capocchi, J. D. T.: Metall. Mater. Trans. A, *31A*, 2000, p. 3137. doi:10.1007/s11661-000-0093-3
[17] Charpentier, M., Daloz, D., Gautier, E., Lesoult, G., Hazotte, A., Grange, M.: Metall. Mater. Trans. A, *34A*, 2003, p. 2139. doi:10.1007/s11661-003-0278-7
[18] Glicksman, M. E.: Principles of Solidification. Springer Science + Business Media, 2011.
[19] Zollinger, J., Daloz, D., Combeau, H.: In: Final Report of Intermetallic Materials Processing in Relation

to Earth and Space Solidification (IMPRESS). Integrated project of European Space Agency, 2004–2009.
[20] Dobrovská, J., Stránský, K., Dobrovská, V.: Acta Metallurgica Slovaca, *13*, 2007, p. 7.
[21] Stalder, I. ., Bilgram, J. H.: Europhys. Lett., *56*, 2001, p. 829. doi:10.1209/epl/i2001-00594-y
[22] Provatas, N., Wang, Q., Haataja, M., Grant, M.: Phys. Rev. Lett., *91*, 2003, article no. 155502. doi:10.1103/PhysRevLett.91.155502
[23] Utter, B., Bodenschatz, E.: Phys. Rev. E, *66*, 2002, article no. 051604. doi:10.1103/PhysRevE.66.051604
[24] Amoorezaei, M., Gurevich, S., Provatas, N.: Acta. Mater., *60*, 2012, p. 657. doi:10.1016/j.actamat.2011.10.006
[25] Trivedi, R., Seetharaman, V., Eshelman, M. A.: Metall. Trans. A, *22A*, 1991, p. 585. doi:10.1007/BF02656826
[26] Klimová, A., Lapin, J.: In: METAL 2012 – International Conference on Metallurgy and Materials, Brno, TANGER 2012.
[27] Brody, H. D., Flemings, M. C.: Trans. Metall. Soc. AIME, *236*, 1966, p. 615.